NMR Structural Determinants of Eosinophil Cationic Protein Binding to Membrane and Heparin Mimetics

María Flor García-Mayoral,[†] Mohammed Moussaoui,[‡] Beatriz G. de la Torre,[§] David Andreu,[§] Ester Boix,[‡] M. Victòria Nogués,[‡] Manuel Rico,[†] Douglas V. Laurents,[†] and Marta Bruix[†*]

[†]Instituto de Química-Física "Rocasolano", CSIC, Madrid, Spain; [‡]Department de Bioquímica i Biología Molecular, Facultat de Biociències, Universitat Autònoma de Barcelona, Barcelona, Spain; and [§]Departament de Ciències Experimentals i de la Salut, Universitat Pompeu Fabra, Barcelona, Spain

ABSTRACT Eosinophil cationic protein (ECP) is a highly stable, cytotoxic ribonuclease with the ability to enter and disrupt membranes that participates in innate immune defense against parasites but also kills human cells. We have used NMR spectroscopy to characterize the binding of ECP to membrane and heparin mimetics at a residue level. We believe we have identified three Arg-rich surface loops and Trp^{35} as crucial for membrane binding. Importantly, we have provided evidence that the interaction surface of ECP with heparin mimetics is extended with respect to that previously described (fragment 34–38). We believe we have identified new sites involved in the interaction for the first time, and shown that the N-terminal α-helix, the third loop, and the first and last β-strands are key for heparin binding. We have also shown that a biologically active ECP N-terminal fragment comprising the first 45 residues (ECP1–45) retains the capacity to bind membrane and heparin mimetics, thus neither the ECP tertiary structure nor its high conformational stability are required for cytotoxicity.

INTRODUCTION

Eosinophil cationic protein (ECP, known also as human ribonuclease 3) is present in large amounts in eosinophil granules. The 3D structure of this 133-residue protein, has been determined with (1) and without ligands by x-ray crystallography (2,3), and recently by NMR spectroscopic methods (4) (Fig. 1). The tertiary structure of ECP closely resembles that of bovine pancreatic ribonuclease A (RNase A) (5), although the loops in ECP are significantly longer. ECP is quite rich in Arg and Pro residues (19 and 12, respectively). ECP has two Trp residues one of which, at position 35, is hyperexposed.

ECP is released by activated eosinophils and at low levels by activated neutrophils (6), and plays a role in host defense against parasites such as helminths (7,8). ECP also inactivates virus (9) and kills both Gram-negative and Gram-positive bacteria at low μM concentrations (10,11). However, ECP can be regarded as a double-edged sword as it is toxic to host epithelial tissues (12,13). In fact, ECP is implicated in asthma (14), the most common childhood disease in developed countries (15). ECP levels in the blood are well correlated with asthma severity and are used widely to monitor the effectiveness of asthma treatments (16).

We are interested in understanding the molecular basis of ECP activities. Previous studies have established that the cytotoxic actions of ECP are mediated chiefly, if not entirely, by its ability to bind and disrupt membranes (17,18), rather than its ribonucleolytic activity, which is 100-fold lower than that of its homolog RNase A (19). More recent studies using Trp fluorescence and site-directed mutagenesis have shown the importance of Trp^{35}, the residues of the third loop 32–39, and the Arg residues in binding to membrane components (18,20,21). These studies, although valuable, do not characterize these interactions directly because they are limited to the environment of the Trp residue and the positions mutated, and site directed mutagenesis may cause structural changes that affect the binding of membrane components in unexpected ways.

A recent study has shown the role of mammalian cell surface glycosaminoglycans, specifically heparin sulfate proteoglycans, in ECP binding and endocytosis (22). It is well known that certain sequence motifs in heparin binding proteins (23) are responsible for the interaction with heparin. Using site-directed mutagenesis and synthetic peptides it was shown that the segment 34–38 of ECP (RWRCK) serves as a specific heparin binding site (22). Nevertheless, these studies were carried out with ECP fragments and the specific heparin binding site of native ECP has not yet been characterized structurally. Interestingly, it has been shown that ECP binds to the glycocalix of eukaryote cells in cellular cultures (17), suggesting that the tight binding to heparin might modulate the cytotoxicity of ECP.

Using NMR spectroscopy, we present a study to structurally characterize all these interactions more completely at a residue level. NMR spectroscopy can, in principle, uncover the participation of all residues in binding without perturbing them. We have used dodecylphosphorylcholine (DPC) micelles as a membrane mimetic, and a disaccharide mimetic of heparin. DPC micelles were chosen because they have zwitterionic character, which is common among lipids present on the outer leaflet of human membranes (24,25). Heparin is a linear, highly sulfated glycosaminoglycan that is released by activated mast cells during inflammatory

Submitted December 18, 2009, and accepted for publication February 26, 2010.

*Correspondence: mbruix@iqfr.csic.es

Editor: Marc Baldus.

0006-3495/10/06/2702/10 $2.00

doi: 10.1016/j.bpj.2010.02.039

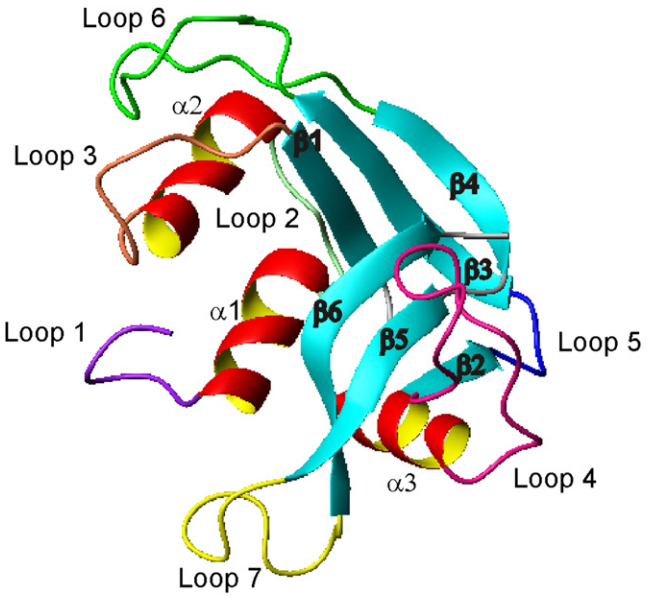

FIGURE 1 Solution structure of ECP. Ribbon display of ECP with secondary structure elements detailed. The molecule is composed of three α-helices and six β-strands connected by different loops colored in purple (loop 1: M0–T6), light green (loop 2: S17–R22), coral (loop 3: N32–N39), magenta (loop 4: G56–N70), blue (loop 5: R75–R77), green (loop 6: I86–R97), and yellow (loop 7: R114–P123).

processes. We chose the disaccharide, 2S sulfated iduronic acid (IdoA) 1-4 linked to 6S and NS sulfated glucosamine (GlcN), as the shortest heparin repeating unit. Heparin-derived disaccharides have been used in the past for this purpose (26), and in some cases benefit has been obtained from their reduced capacity to induce aggregation (27).

ECP has an exceptionally high conformational stability; it is ~3.5 kcal/mol more stable than RNase A (4,28,29). Because conformational stability was shown to be a determinant of cytotoxicity in a series of RNase A variants (30), this high conformational stability was thought to play a role in the cytotoxicity of ECP. However, work on both a cytotoxic RNase from chickens with Arg-rich loops (31), and more recently, human ECP (32), has shown that peptides derived from these proteins also possess potent cytotoxic activities in the absence of stable tertiary structure. To better understand the relationship between stability, structure, and activity, we study the conformation of a cytotoxic ECP peptide (residues 1–45) by NMR spectroscopy.

MATERIALS AND METHODS

Materials

Dodecylphosphorylcholine-d_{38} (98% atom D) (DPC) was an Isotec product obtained from Sigma-Aldrich (Madrid, Spain). The heparin sulfate disaccharide, IdoA (2S) 1-4 linked to GlcNS (6S), was obtained from Sigma-Aldrich (heparin disaccharide I-S sodium salt). 2,2,2-Trifluoroethanol-d_3 (TFE) (>99.5% pure, NMR spectroscopy grade) was purchased from Sigma-Aldrich.

Peptide synthesis

The peptide sample containing the first 45 N-terminal residues of ECP (ECP1–45) was chemically synthesized by Fmoc solid phase procedures and purified by high performance liquid chromatography to 95% purity. Cys residues at positions 23 and 37 in the native sequence were replaced by Ser to avoid potential formation of inter- or intramolecular disulfide bridges. The identity and sequence of the peptide was confirmed by matrix assisted laser desorption/ionization time-of-flight mass spectrometry and NMR spectroscopy.

Purification of recombinant ^{15}N-ECP

The protein was expressed in *Escherichia coli* BL21(DE3) cells in minimal medium with $^{15}NH_4Cl$ as the sole source for nitrogen and purified from inclusion bodies as described previously (33).

NMR samples

All NMR samples were recorded at 25°C, pH 4.5 and contained 50 μM of DSS as the internal chemical shift reference.

ECP samples

A ~0.5 mM sample of ^{15}N-ECP was initially prepared in 90% H_2O/10% D_2O. Analogous aqueous solution samples of ^{15}N-ECP were then prepared in deuterated DPC micelles, heparin sulfate disaccharide, and in the presence of both DPC and heparin sulfate. The final concentrations were ~0.5 mM ^{15}N-ECP and ~40 mM DPC for the sample containing DPC; ~0.25 mM ^{15}N-ECP and ~0.25 mM heparin sulfate (1:1 complex) for the sample with the disaccharide; and ~0.5 mM ^{15}N-ECP, ~40 mM DPC, and ~0.5 mM heparin sulfate for the sample with the three compounds present.

ECP1-45 peptide samples

The initial sample of ~1.1 mM ECP1-45 peptide was prepared in aqueous solution of 90% H_2O/10% D_2O. Three subsequent samples of ~1.1 mM ECP1–45 peptide in the same aqueous solution were prepared in 40% TFE, 20 mM DPC micelles, and 20 mM DPC plus ~1 mM heparin sulfate disaccharide, respectively. A fourth sample of ECP1–45 in 1:1 complex with heparin sulfate disaccharide alone was prepared at concentration of ~2.5 mM. Another ~1.1 mM sample of the peptide was prepared in D_2O solution to evaluate amide proton exchange rates with the solvent. The final pH reading for this sample was 4.5, with no correction for the isotope effect.

Heparin sulfate disaccharide sample

A 1.6-mM sample of heparin sulfate disaccharide in D_2O pH 4.5 was used to record NMR spectra for the assignment of this molecule.

NMR experiments

Series of 2D correlation spectroscopy (COSY), nuclear Overhauser effect spectroscopy (NOESY), and total correlation spectroscopy (TOCSY) spectra were acquired in a Bruker Avance 800 MHz spectrometer equipped with a *z*-gradient cryoprobe at 25°C. Standard pulse sequences were used. Mixing times were 150 ms and 60 ms for NOESY and TOCSY experiments recorded for ECP1–45, and 100 ms and 60 ms respectively for the ^{15}N-ECP sample. The same set of experiments were recorded in the heparin sulfate disaccharide sample with mixing times of 200 ms and 60 ms for 2D NOESY and TOCSY spectra, respectively. The spectra were processed with Topspin 1.3 (Bruker, Rheinstetten, Germany) and transferred to Sparky (34) for further analysis. MolMol was used for molecular display (35).

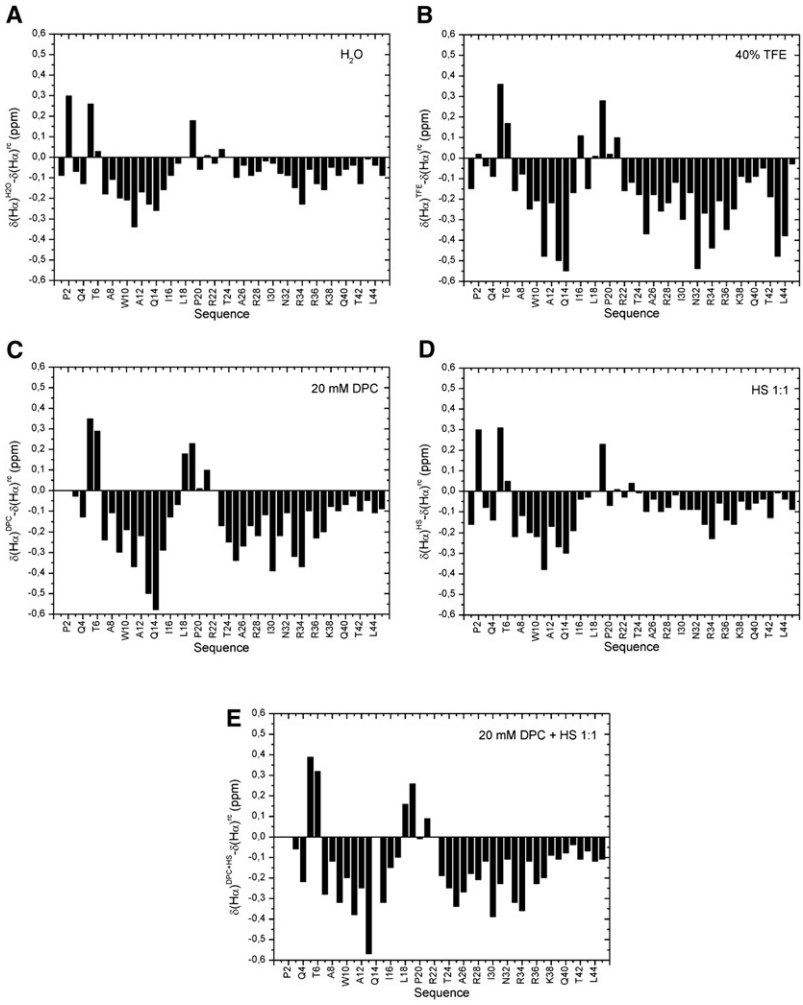

FIGURE 2 Conformational chemical shifts of ECP1–45 peptide: $\Delta\delta$ values for $^1H\alpha$ protons at pH 4.5 and 25°C are represented for the five different environments studied: (*A*) aqueous solution; (*B*) 40% TFE; (*C*) 20 mM DPC; (*D*) heparin sulfate disaccharide (1:1 complex with ECP1–45); and (*E*) 20 mM DPC + heparin disaccharide (1:1 complex with ECP1–45).

Estimation of helix populations-

Helix populations were quantified from the $^1H\alpha$ conformational chemical shift (CCS) values as described (36). Thus, the $\Delta\delta_{H\alpha}$ differences ($\Delta\delta_{H\alpha} = \delta_{H\alpha}{}^{observed} - \delta_{H\alpha}{}^{random\ coil}$, ppm) averaged for all the helical residues were divided by the $\Delta\delta_{H\alpha}$ value corresponding to 100% helix, −0.39 ppm (37), and then multiplied by 100.

RESULTS

The ^1H NMR resonances of ECP and the peptide ECP1–45 in the different environments, TFE, DPC, and heparin sulfate disaccharide were assigned using the standard procedures (38). The assignments are essentially complete except for a few isolated residues in the presence of DPC due to spectral overlap or broadening.

ECP1–45 in water solution

We have used CCS of $^1H\alpha$ protons to assess the secondary structure content of the peptide in the different environments tested (37). As shown in Fig. 2 *A*, the peptide in aqueous solution is mainly unstructured and displays a low propensity to form two α-helices spanning approximately residues R7–S17 and I25–R45. The boundaries of the first helix match those of native helix α1 of ECP. However, the second helix has remarkably lengthened the native helix α2 (C23–N31) at its C-terminus by incorporating residues in loop 3 (N32–N39) and strand β1 (Q40–R45) of native ECP. The helix populations are calculated to be 47% and 21% for the first and second helices, respectively. Very few and weak sequential ^1HN-^1HN nuclear Overhauser effects (NOEs) were observed. The chemical shifts of the ^1H side chains are in the range of unstructured peptides and no evidence for native or nonnative clusters are seen. In agreement with these results, the 1D ^1H NMR spectrum recorded at 25°C, pH 4.5 in a D_2O sample, showed essentially complete exchange of all amide hydrogens, providing evidence that the protection afforded by helical structure of ECP1–45 against exchange is very weak.

ECP1–45 in TFE

The conformation of ECP1–45 was studied in 40% TFE solution because it bears some resemblance to membrane environments (39). The $^1H\alpha$ CCS values show a significant increase in the α-helical propensity. The boundaries for the

two helices are comparable to those in water solution, and notably the second helix is also longer in 40% TFE. The estimated helical populations are 76% for the first helix and 63% for the second (Fig. 2 *B*); these values are 1.5- and 3-fold higher than their populations in aqueous solution. In addition to the $^1H\alpha$ CCS values, the much higher tendency to form the two helices is reflected by: 1), changes in ^1HN $\Delta\delta >$ 0.15 ppm for most residues in these segments; 2), an increase in the number and intensities of sequential ^1HN-^1HN NOEs especially in the segments Q4–I16 and T24–L44; and 3), the observation of some unequivocal nonoverlapped $^1H\alpha$-^1HN (i, i + 3) NOEs characteristic of helical conformation like those between A8–F11, W10–I13 in the first helix, and R28–N31, I30–Y33, W35–K38 in the second helix.

ECP1–45 in DPC micelles

The conformation of ECP1–45 was studied in 20 mM DPC, which forms small uniform micelles that tumble rapidly enough for solution NMR spectroscopy, and mimic more realistically the membrane environment (40). As in 40% TFE, the $^1H\alpha$ CCS values (Fig. 2 *C*) of ECP1–45 in the presence of DPC micelles also show a significantly increased tendency to form the two α-helices as compared to the aqueous medium, with estimated helical populations of 71% and 47% for the first and second helices, respectively. In the presence of DPC, residues N32–L44 also adopt a helical conformation that extends native helix α2. Despite the spectral line broadening induced by decreased mobility of the complex, the backbone assignment is complete with the exception of the $^1H\alpha$ of R22. The poorer quality of the spectra made it more difficult to identify ($^1H\alpha$-^1HN i, i + 3) helical NOEs, however, those between W10–I13 in the N-terminal helix, and N31–R34 and N32–W35 in the central part of the C-terminal helix could be unambiguously assigned. Thirteen ^1HN-^1HN NOE connections: R7–A8, A8–Q9, Q9–W10, F11–A12, Q14–H15, H15–I16, I30–N31, R34–W35, R36–S37, Q40–N41, N41–T42, T42–F43, and F43–L44 are observed. The chemical shift perturbation (CSP) analysis shows changes >0.15 ppm for the ^1HN protons of R7, Q9, F11, H15, I16, S17, L18, A26, A29, I30, R34, W35, K38, N39, and F43, and the $^1H\alpha$ of T6, I13, Q14, L18, S23, T24, I25, A26, I30, Y33. Some side-chain protons also experience important $\Delta\delta$ (0.15–0.35 ppm), for example, those of W10, Q14, H15, N32, and W35 to mention a few examples; Arg side chains are also greatly perturbed.

ECP1–45 interaction with Heparin mimetic

Previous studies have established the ability of ECP to interact with glycosaminoglycan structures, in particular heparin (41). The heparin disaccharide resonances were assigned and the measured chemical shifts are in agreement with the reported values (42).

Spectra of ECP1–45 in the presence of the heparin sulfate disaccharide are quite similar to those in water solution, with a low tendency to form two α-helices (Fig. 2 *D*). The percentages of the helical contents are comparable to those obtained in aqueous solution, with values of 50% and 24% for the first and second helices, respectively. The boundaries for both helices are similarly retained. Despite these similarities, the NMR data provide conclusive evidence for the binding of the peptide and the disaccharide, the sign of the disaccharide intramolecular NOEs changes from positive in the spectra registered in the absence of ECP1–45 to negative in its presence due to their different tumbling regimes (Fig. 3). Because the free disaccharide is a small and fast rotating molecule, the NOEs have the opposite sign relative to the diagonal peaks. However, when the interaction with the peptide occurs, the different diffusional properties of the larger complex are reflected in the sign of the NOEs that are now the same as the diagonal.

No large CSPs are detected for the peptide resonances in the presence of the disaccharide or for the disaccharide resonances in the presence of the peptide. Accordingly, no important changes in the peptide NOEs are observed indicating that carbohydrate-induced conformational changes are small. Additionally, no intermolecular NOEs could be detected, indicating the highly dynamic nature of the complex interface, which promotes NOE quenching and makes their NMR detection difficult (43,44). The two sets of resonances corresponding to the α and β conformers of the GlcN unit are still observed in the presence of the peptide, indicating that no preferential conformer is trapped when the complex is formed. CSPs are small for ^1HN and $^1H\alpha$ protons; values >0.025 ppm are observed for the ^1HN of F5, T6, R7, Q9, W10, F11, A12, Q14, H15, I16, S17, L18, R28, I30, N32, and K38, and the $^1H\alpha$ of F5, R7, F11, I13, Q14, H15, I16, I30, and N32. Residues from R34 to N39 have been suggested to participate in the interaction of native ECP with heparin based on characteristic patterns of basic and hydrophobic residues observed in glycosaminoglycan interacting proteins and also identified in loop 3 of eosinophil-derived neurotoxin (22). In addition, residues from the N-terminal helix of ECP and Q14 at the active site have been proposed to mediate the interaction based on docking simulations (45). The chemical shifts of the aromatic side chains of F5, F11, Y33, and W35 are similar to those in water solution lacking the heparin disaccharide, as are the side chains of the remaining residues in the segment R34-N39. In contrast, the $^1H\varepsilon3$ proton of W10 is clearly shifted toward higher field ~0.05 ppm, and the ^1H chemical shift values of Qγ, Hε21, and Hε22 of Q14 are shifted upfield ~0.08, 0.13, and 0.04 ppm, respectively, suggesting the implication of these side chains in the interaction.

ECP1–45 in DPC micelles and heparin sulfate disaccharide

To investigate whether the high affinity interaction of ECP1–45 with heparin sulfate disaccharide displaces the

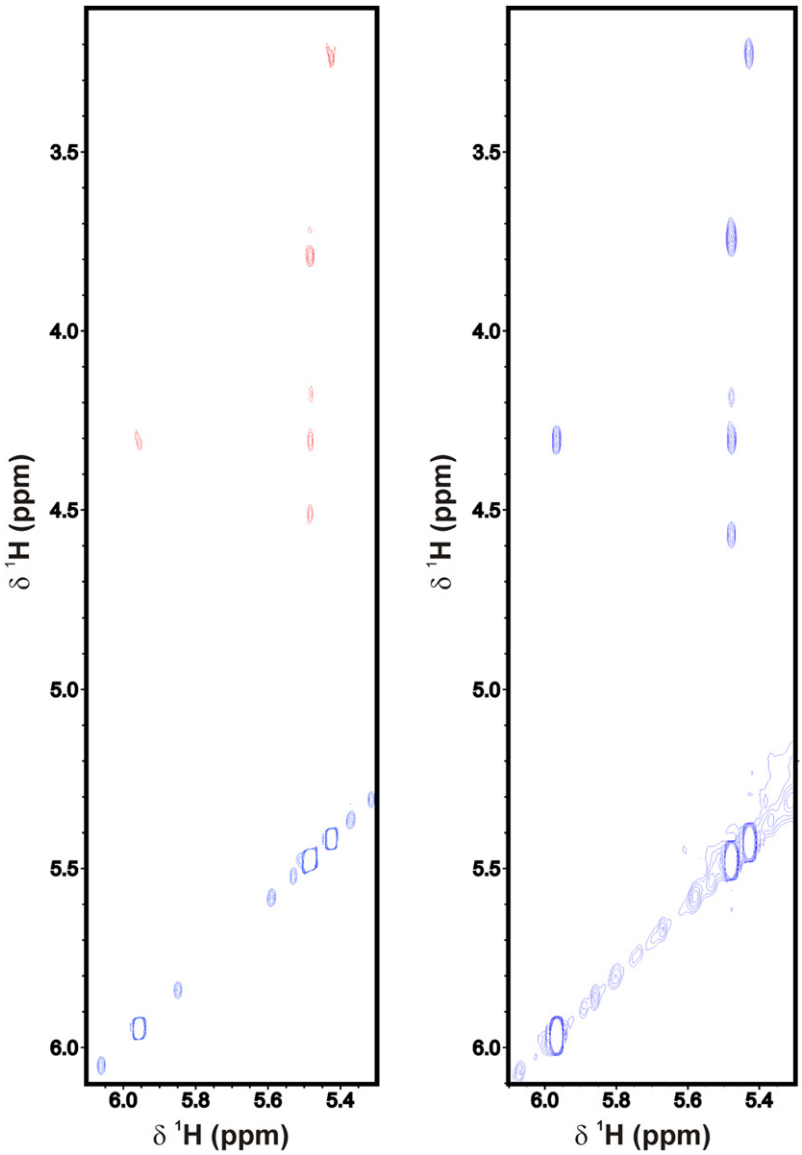

FIGURE 3 ECP1–45 binding to disaccharide heparin mimetic. Anomeric region of the 2D NOESY spectra recorded in (*left*) the absence and (*right*) the presence of the ECP1–45 peptide. (*left*) The different sign of the free disaccharide NOEs (*red*) with respect to the diagonal of the spectrum (*blue*) is characteristic of small and fast rotating molecules. (*right*) The same sign of the bound disaccharide NOEs (*blue*) with respect to the diagonal (*blue*), reflects the diffusional properties of the larger complex when the interaction with the peptide occurs.

interaction with DPC, which would indicate common/partially superimposing interfaces, we added the disaccharide to our previous sample in DPC solution. The spectra showed the broad resonances characteristic of the peptide-micelle complex, and the spectra could be easily assigned using ECP1–45 assignments in DPC micelles. The ^{1}Hαs of Q14 and R22 could not be identified. The CCSs are similar to those in the DPC medium alone (percentages of 71% and 47% for both helices, Fig. 2 *E*), thus the increased helix population induced by DPC is not reduced by adding the heparin mimetic. The chemical shift differences provoked in ECP1–45 by the disaccharide in the presence of DPC are similar to those detected in the absence of DPC. In general, the CSPs are small, with chemical shift changes >0.025 ppm occurring for ^{1}HN protons of residues Q4, F5, A8, W10, F11, I13, H15, T24, I30, and N32, and ^{1}Hα of P3, Q4, F5, T6, R7, A12, I13, H15, S17, and N19. Significant chemical shift changes are found for the ^{1}Hε1, ^{1}Hδ1, and ^{1}Hε3 of W10 (0.05, 0.05, 0.09 ppm, respectively). These changes match those observed with the disaccharide alone quite well, suggesting that the interaction surfaces with DPC and heparin are not mutually exclusive.

ECP interaction with DPC micelles

Next, ^{15}N-HSQC spectra of native, full length, ^{15}N-labeled ECP in aqueous solution (Fig. 4 *A*) and in DPC micelles (Fig. 4 *B*) were recorded and assigned based on recently published data (4) and corroborated at these solvent conditions using 3D ^{15}N-NOESY-HSQC spectra. Using the CSPs induced in ^{1}HN and ^{15}N chemical shifts on binding to DPC, we have mapped the residues most affected on the molecule surface (Fig. 5, *A* and *B*). The interaction surface is well defined and constituted by residues belonging to

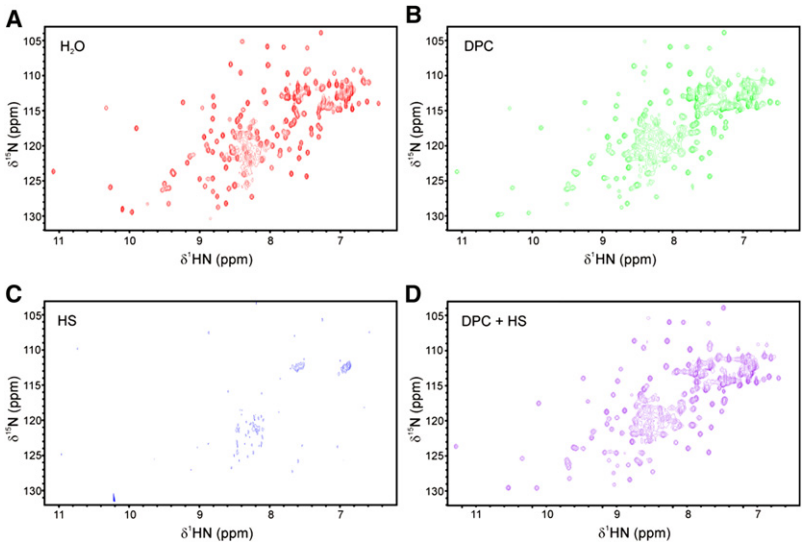

FIGURE 4 ^{15}N-HSQC spectra of native ECP, pH 4.5 and 25°C, in different conditions. (*A*) Aqueous solution and the presence of (*B*) 40 mM DPC, (*C*) heparin sulfate disaccharide (1:1 complex), and (*D*) 40 mM DPC and heparin sulfate disaccharide (1:1 complex).

different loops, Q4-T6 in loop 1, N32-R36 in loop 3, T46 in the segment connecting strand β1 with helix α3, and N87, A90-I93, C96, R97 in loop 6. The ^{1}Hε1 side-chain proton of W35 experiences one of the largest variations observed in the HSQC spectrum corroborating its crucial role in the process. These three protein loops project outward on the same face of the molecule with residues in loop 3 stacked in between loops 1 and 6. W35 side chain is hyperexposed, which facilitates its insertion into the micelle and stabilization of the complex interface environment (46).

ECP interaction with heparin mimetic in the presence of DPC micelles

ECP strongly interacts with heparin sulfate oligosaccharides (22). At concentrations suitable for NMR spectroscopy, we observed that the ECP sample precipitated instantly on adding the heparin sulfate disaccharide, which thwarted efforts to characterize their complex under these conditions. The ^{15}N-HSQC spectrum of this sample (Fig. 4 *C*) indicates that no native ECP is left in solution. Therefore, the disaccharide was added to a sample containing ECP and DPC. No precipitation was observed, and the effects of the addition of the disaccharide were analyzed by the chemical shift changes induced in the ^{15}N-HSQC spectrum of ECP recorded in these conditions with respect to the DPC solution alone (Fig. 4 *D*). By using the average ^{1}HN and ^{15}N chemical shift values to map the interaction surface, the biggest perturbations were found to affect residues Q4 in loop 1, A8 and F11-Q14 in helix α1, Y33-R36 in loop 3, Q40-L44 in strand β1, C62, H64, R66 in loop 4, R75, R77 in loop 5, C83, L85 in strand β3, and H128-D130 in strand β6 (Fig. 5, *C* and *D*). The side chain ^{1}Hε1 protons of W10 and W35 are also considerably perturbed (0.11 and 0.14 ppm, respectively). CSPs implicate a large number of Arg residues in binding the disaccharide; Arg residues are common at heparin binding domains due to their hydrogen bonding propensity and strong electrostatic interactions with sulfate groups (47). Although residues in loop 3 are common to the interaction surface with DPC, residues in the C-terminal part of the first helix are exclusively perturbed by the disaccharide, most notable the catalytically relevant residue Q14, whereas loop 1 is affected selectively by DPC binding.

DISCUSSION

Despite recent progress, we are still far from understanding completely the mechanism of action of cytotoxic RNases. The elucidation of their activities requires structural studies with targets. To characterize the structural bases of the cytotoxic activity related to ECP interaction with membranes, we have used NMR to study the behavior of ECP and the N-terminal-derived peptide ECP1–45 in water and in media that mimic the membrane environment of eukaryote cells. Residues 1–45 of ECP were detected by an algorithm as having a high propensity to be bactericidal (48) and were shown to maintain most of the membrane-destabilizing and antimicrobial activities of ECP (32). This suggests that this segment probably constitutes the main functional domain of ECP.

ECP1–45 conformational preferences and binding to DPC membrane mimetic

We have studied the ECP1–45 peptide to gain insight into the relationships between structure, stability and biological activities of ECP. Secondary chemical shifts and H/D exchange data provide clear evidence that the ECP1–45 peptide, although mainly unstructured in water, forms two partially populated α-helices separated by a flexible turn (L18–T24). Because the conformational restraint imposed by the disulfide bridge C37–C96 of native ECP is not present in the peptide, the substitution of C37 by S37 may allow the second helix to become longer. The second helix is less

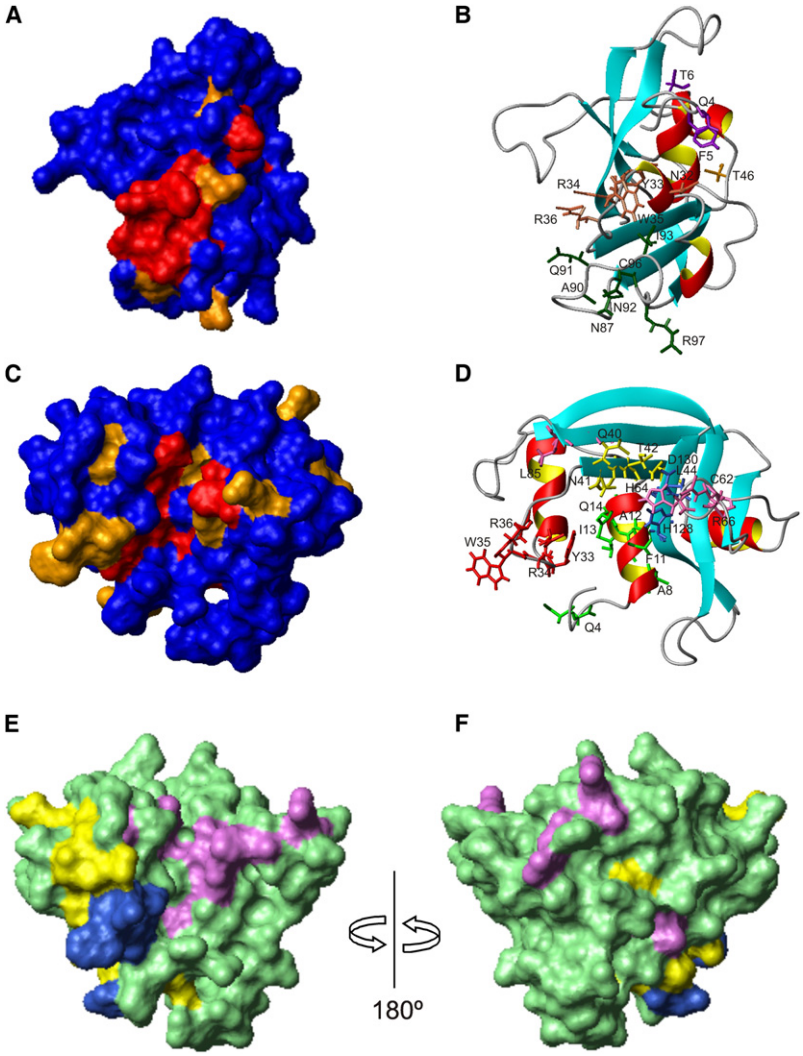

FIGURE 5 Interaction surfaces of native ECP with DPC and heparin mimetic. (*A*) Chemical shift perturbation map for DPC displayed on the surface of ECP; red $\Delta\delta >$ 0.08 ppm, orange $0.05 < \Delta\delta < 0.08$. (*B*) Residues involved in the interaction of ECP with DPC are colored according to the groups described in the text, loop 1 (*violet*), loop 3 (*coral*), and loop 6 (*green*). (*C*) Chemical shift perturbation map for heparin disaccharide displayed on the molecular surface of ECP; red $\Delta\ \delta > 0.08$ ppm, orange $0.05 < \Delta\delta < 0.08$ ppm. (*D*) Residues involved in the interaction of ECP with heparin sulfate disaccharide are colored according to the groups described in the text, A8–Q14 (*green*), Y33–R36 (*red*), Q40–L44 (*yellow*), H128–D130 (*blue*). Other affected residues are pink. (*E* and *F*) Simultaneous representation of the interaction surface of ECP with DPC and heparin mimetic. Residues in blue are common to the interaction with DPC and heparin disaccharide, residues in yellow belong exclusively to the interaction surface with DPC, and residues in violet correspond exclusively to the interaction surface with heparin sulfate disaccharide.

populated in all the environments studied, although its helical content rises substantially in 40% TFE and DPC micelles. An overall increase in helical structure was also observed by CD spectroscopy for ECP1–45 in the presence of SDS micelles or bacterial membrane components (32). Interestingly, the adopted helix-turn-helix motif is common in many peptides that interact with membranes, including a variety of antimicrobial peptides (49–51).

Previous studies have already identified some residues in the fragment 1–45 as important for the interaction with membranes. In particular, the highly solvent-exposed W35 and nearby arginine residues, R34 and R36, participate actively in membrane interactions. By NMR, we corroborate that these residues are involved, and we also find additional residues participating in membrane interactions. Most form clusters of positively charged and aromatic residues (R7, F11, H15, in helix α1, and R34, W35, K38, F43 in helix α2) and aliphatic chains (A26, A29, I30 in helix α2) that are concentrated on opposite helical faces. This orientation suggests that they are favorably positioned to form electrostatic and hydrophobic interactions with the membrane (52).

Insights into the capacity of ECP to bind and disrupt membranes

Our NMR analysis shows that the interaction surface of ECP with DPC micelles is well-defined, involving loops 1 (R1–T6), 3 (N32–N39), and 6 (I86–R97) in the interactions (Fig. 5, *A* and *B*). These three loops point toward the same face of the protein; loop 3 is sandwiched by loops 1 and 6 in a spatial disposition that may strengthen binding. Some Gln and Asn side chains (Q4, N32, Q91) and many Arg side chains have high degrees of solvent exposure and are likely to be involved in H-bond formation. For example, R97 is also solvent exposed and could assist Args in loop 3 to bind DPC micelles. Interestingly, R97 corresponds to the only polymorphism known. The R97T variant implies a new glycosylation site and this variant is markedly less cytotoxic (46). On enzymatic deglycosylation, the R97T

variant recovers its cytotoxicity, suggesting that glycosylation can cover a key region for cytotoxicity (21). Recent studies suggest that ECP activity is enhanced by deglycosylation during eosinophil activation (53). Nitration of tyrosines is another posttranslational modification recently identified for eosinophil secretory proteins and associated with eosinophil maturation. Tyr nitration occurs in ECP exclusively on Y33 (54) and may modify its interacting properties. The aromatic ring of Y33 is expected to contribute modestly to membrane binding as it is buried in some NMR structures (4). Nitration likely favors the more exposed conformation of Y33 seen in other NMR solution structures and could position it to interact favorably with positively charged choline moieties in membranes.

The groove between helix α1 and loop 3 of ECP can accommodate heparin mimetics

The oligomerization of heparin-binding proteins on the heparin chain is a common event (55,56). The observed sample precipitation when ECP was mixed with a solution containing the heparin sulfate disaccharide precluded the study of the interaction between full-length ECP and the heparin disaccharide. Instead, ECP1–45 plus disaccharide, and ECP in DPC micelles plus this disaccharide were studied. The binding to ECP1–45 is in general agreement with that observed for ECP, although we also found important differences. Residues in the stretch Q9–H15 participate in binding in both ECP and ECP1–45, however, no significant changes occur in the peptide for residues in loop 3 of ECP. Among the aromatic groups, F5, W10, and F11 are implicated in binding. R7, W10, F11, Q14, and H15 are mainly localized on one face of the first helix. It is conceivable that the aromatic residues in this stretch, together with F5 probably playing the role of W35 in native ECP, form a hydrophobic platform in one side of the helix. R7 can contribute electrostatically to the interaction. Because ECP1–45 retains nearly all of the bactericidal activity of the whole protein, the differences noted above may account primarily for the partially retained membrane depolarization capacity of the peptide (32). This data also indicates that the tertiary structure of ECP and remarkably high conformational stability are not required for these functions. Therefore the real physiological role of the remarkably high conformational stability of ECP is a mystery. As a working hypothesis for designing future studies, we suggest that the high conformational stability of ECP might be required for storage in eosinophil granules.

Concerning ECP, the residues identified to be involved directly or indirectly in heparin binding can be grouped into four main groups shown in Fig. 5, *C* and *D*: 1), A8–Q14 in helix α1; 2), Y33–R36 in loop 3; 3), Q40–L44 in strand β1; and 4), H128–D130 in strand β6. Whereas the interaction of residues in loop 3 of ECP with heparin mimetics was described previously (22), those in the other three groups have been identified in this study for what we believe to be the first time. Examining these results in the context of the ECP solution structure, we are able to propose a model for the interaction. Residues in loop 3 of ECP, are spatially close to the second half of helix α1, and these two regions face each other defining a groove that would accommodate the sugar moiety. This groove is bound on top by residues in strand β1. The opposite face of the helix α1 is close to residues of strand β6.

Two Trp residues (W10 and W35) are found in the groups mentioned above. As W35 is highly solvent-exposed whereas W10 is mainly buried, it is expected that the W35 contribution to the binding affinity will be higher. The two Arg residues adjacent to W35 probably contribute to the binding affinity by ion-pairing spatially with negatively charged sulfate or carboxylate groups of the disaccharide. Such interactions are common for Arg-rich membrane penetrating peptides (57). The side chains of W10, Q14, and Y33 are near each other and oriented toward the interior of the cavity. Actually, the perturbation observed for the ^{1}HN of Q14 is one of the largest in the spectra suggesting that this residue is involved in the binding process. In ECP, Q14 is close to N41 and F43; this would explain the perturbations observed for residues in strand β1. F11 is on the side of the helix pointing away from the cavity and toward residues in strand β6, and in particular its side chain is near that of L129, which is also near strand β1. These contacts suggest an explanation for the changes in this region.

Some of the residues that we have found to participate in the binding of ECP to heparin disaccharide (Q14, Q40, T42, L129) are located at RNA substrate binding sites. Among the catalytic residues, H128 seems to participate in disaccharide binding. Consequently some of the residues involved in the ribonucleolytic activity of ECP also participate in ECP binding to heparin, and this can account for the decreased ribonucleolytic activity with increasing heparin concentrations (45).

Interestingly the set of residues in the protein surface that are in contact with heparin disaccharide only partly overlap that involved in DPC interactions (Fig. 5, *E* and *F*). Because the broadening of the NMR signals resulting from the formation of the large complex of ECP with the micelles is retained when the heparin disaccharide is present, and also additional chemical shift perturbations are observed (particularly those in helix α1), it is likely that ECP binds to membranes and heparin simultaneously. This could have implications for the efficient internalization of ECP in membranes (57), host cytotoxicity, and its ability to modulate the immune system. The residues binding to DPC micelles, which mimic the outer leaflet of human membranes, are largely those that are also implicated in binding to bacterial membrane and cell wall components (58). This suggests that it will be difficult to engineer ECP variants that do not harm host cells yet retain potent toxicity for parasites, bacteria, and virus.

This work was supported by the Spanish Ministerio de Ciencia e Innovación (CTQ2008-00080/BQU, BIO2008-04487-CO3-02, BFU2006-15543-CO2-01, BFU2009-09371).

REFERENCES

1. Mohan, C. G., E. Boix, …, K. R. Acharya. 2002. The crystal structure of eosinophil cationic protein in complex with 2′,5′-ADP at 2.0 A resolution reveals the details of the ribonucleolytic active site. *Biochemistry*. 41:12100–12106.
2. Boix, E., D. D. Leonidas, …, K. R. Acharya. 1999. Crystal structure of eosinophil cationic protein at 2.4 A resolution. *Biochemistry*. 38:16794–16801.
3. Mallorquí-Fernández, G., J. Pous, …, M. Coll. 2000. Three-dimensional crystal structure of human eosinophil cationic protein (RNase 3) at 1.75 A resolution. *J. Mol. Biol.* 300:1297–1307.
4. Laurents, D. V., M. Bruix, …, M. Rico. 2009. The (1)H, (13)C, (15)N resonance assignment, solution structure, and residue level stability of eosinophil cationic protein/RNase 3 determined by NMR spectroscopy. *Biopolymers*. 91:1018–1028.
5. Santoro, J., C. González, …, M. Rico. 1993. High-resolution three-dimensional structure of ribonuclease A in solution by nuclear magnetic resonance spectroscopy. *J. Mol. Biol.* 229:722–734.
6. Monteseirín, J., A. Vega, …, J. Conde. 2007. Neutrophils as a novel source of eosinophil cationic protein in IgE-mediated processes. *J. Immunol.* 179:2634–2641.
7. McLaren, D. J., C. G. Peterson, and P. Venge. 1984. Schistosoma mansoni: further studies of the interaction between schistosomula and granulocyte-derived cationic proteins in vitro. *Parasitology*. 88:491–503.
8. Hamann, K. J., G. J. Gleich, …, R. L. Barker. 1990. In vitro killing of microfilariae of *Brugia pahangi* and *Brugia malayi* by eosinophil granule proteins. *J. Immunol.* 144:3166–3173.
9. Domachowske, J. B., K. D. Dyer, …, H. F. Rosenberg. 1998. Eosinophil cationic protein/RNase 3 is another RNase A-family ribonuclease with direct antiviral activity. *Nucleic Acids Res*. 26:3358–3363.
10. Lehrer, R. I., D. Szklarek, …, G. J. Gleich. 1989. Antibacterial properties of eosinophil major basic protein and eosinophil cationic protein. *J. Immunol.* 142:4428–4434.
11. Boix, E., M. Torrent, …, M. V. Nogués. 2008. The antipathogen activities of eosinophil cationic protein. *Curr. Pharm. Biotechnol*. 9:141–152.
12. Fredens, K., R. Dahl, and P. Venge. 1982. The Gordon phenomenon induced by the eosinophil cationic protein and eosinophil protein X. *J. Allergy Clin. Immunol*. 70:361–366.
13. Young, J. D., C. G. Peterson, …, Z. A. Cohn. 1986. Mechanism of membrane damage mediated by human eosinophil cationic protein. *Nature*. 321:613–616.
14. Munthe-Kaas, M. C., J. Gerritsen, …, K. L. Carlsen. 2007. Eosinophil cationic protein (ECP) polymorphisms and association with asthma, s-ECP levels and related phenotypes. *Allergy*. 62:429–436.
15. Woolcock, A. J., and J. K. Peat. 1997. Evidence for the increase in asthma worldwide. *Ciba Found. Symp*. 206:122–134, discussion 134–129, 157–129.
16. Koh, G. C., L. P. Shek, …, D. S. Koh. 2007. Eosinophil cationic protein: is it useful in asthma? A systematic review. *Respir. Med*. 101:696–705.
17. Navarro, S., J. Aleu, …, M. V. Nogués. 2008. The cytotoxicity of eosinophil cationic protein/ribonuclease 3 on eukaryotic cell lines takes place through its aggregation on the cell membrane. *Cell. Mol. Life Sci*. 65:324–337.
18. Carreras, E., E. Boix, …, M. V. Nogués. 2003. Both aromatic and cationic residues contribute to the membrane-lytic and bactericidal activity of eosinophil cationic protein. *Biochemistry*. 42:6636–6644.
19. Sorrentino, S., and D. G. Glitz. 1991. Ribonuclease activity and substrate preference of human eosinophil cationic protein (ECP). *FEBS Lett*. 288:23–26.
20. Carreras, E., E. Boix, …, M. V. Nogués. 2005. Surface-exposed amino acids of eosinophil cationic protein play a critical role in the inhibition of mammalian cell proliferation. *Mol. Cell. Biochem.* 272:1–7.
21. Trulson, A., J. Byström, …, P. Venge. 2007. The functional heterogeneity of eosinophil cationic protein is determined by a gene polymorphism and post-translational modifications. *Clin. Exp. Allergy*. 37:208–218.
22. Fan, T. C., S. L. Fang, …, M. D. Chang. 2008. Characterization of molecular interactions between eosinophil cationic protein and heparin. *J. Biol. Chem.* 283:25468–25474.
23. Cardin, A. D., and H. J. Weintraub. 1989. Molecular modeling of protein-glycosaminoglycan interactions. *Arteriosclerosis*. 9:21–32.
24. Matsuzaki, K. 2009. Control of cell selectivity of antimicrobial peptides. *Biochim. Biophys. Acta*. 1788:1687–1692.
25. Verkleij, A. J., R. F. Zwaal, …, L. L. van Deenen. 1973. The asymmetric distribution of phospholipids in the human red cell membrane. A combined study using phospholipases and freeze-etch electron microscopy. *Biochim. Biophys. Acta*. 323:178–193.
26. Murphy, J. W., Y. Cho, …, E. Lolis. 2007. Structural and functional basis of CXCL12 (stromal cell-derived factor-1 alpha) binding to heparin. *J. Biol. Chem.* 282:10018–10027.
27. Sue, S. C., J. R. Brisson, …, W. Wu. 2001. Structures of heparin-derived disaccharide bound to cobra cardiotoxins: context-dependent conformational change of heparin upon binding to the rigid core of the three-fingered toxin. *Biochemistry*. 40:10436–10446.
28. Maeda, T., K. Mahara, …, H. Yamada. 2002. RNase 3 (ECP) is an extraordinarily stable protein among human pancreatic-type RNases. *J. Biochem.* 132:737–742.
29. Nikolovski, Z., V. Buzón, …, M. V. Nogués. 2006. Thermal unfolding of eosinophil cationic protein/ribonuclease 3: a nonreversible process. *Protein Sci*. 15:2816–2827.
30. Klink, T. A., and R. T. Raines. 2000. Conformational stability is a determinant of ribonuclease A cytotoxicity. *J. Biol. Chem.* 275:17463–17467.
31. Nitto, T., K. D. Dyer, …, H. F. Rosenberg. 2006. Evolution and function of leukocyte RNase A ribonucleases of the avian species, *Gallus gallus*. *J. Biol. Chem.* 281:25622–25634.
32. Torrent, M., B. G. de la Torre, …, E. Boix. 2009. Bactericidal and membrane disruption activities of the eosinophil cationic protein are largely retained in an N-terminal fragment. *Biochem. J.* 421:425–434.
33. Boix, E., Z. Nikolovski, …, M. V. Nogués. 1999. Kinetic and product distribution analysis of human eosinophil cationic protein indicates a subsite arrangement that favors exonuclease-type activity. *J. Biol. Chem.* 274:15605–15614.
34. Goddard, T. D., and D. G. Kneller. 2005. Sparky 3. University of California, San Francisco, CA.
35. Koradi, R., M. Billeter, and K. Wüthrich. 1996. MOLMOL: a program for display and analysis of macromolecular structures. *J. Mol. Graph.* 14:51–55, 29–32.
36. Jiménez, M. A., M. Bruix, …, M. Rico. 1993. CD and ^{1}H-NMR studies on the conformational properties of peptide fragments from the C-terminal domain of thermolysin. *Eur. J. Biochem.* 211:569–581.
37. Wishart, D. S., B. D. Sykes, and F. M. Richards. 1991. Relationship between nuclear magnetic resonance chemical shift and protein secondary structure. *J. Mol. Biol.* 222:311–333.
38. Wüthrich, K. 1986. NMR of Proteins and Nucleic Acids. Wiley-InterScience, John Wiley and Sons, New York, NY.
39. Luo, P., and R. L. Baldwin. 1997. Mechanism of helix induction by trifluoroethanol: a framework for extrapolating the helix-forming properties of peptides from trifluoroethanol/water mixtures back to water. *Biochemistry*. 36:8413–8421.
40. McDonnell, P. A., and S. J. Opella. 1993. Effect of detergent concentration on multidimensional solution NMR spectra of membrane proteins in micelles. *J. Magn. Reson.* 102:120–125.
41. Maeda, T., M. Kitazoe, …, M. Seno. 2002. Growth inhibition of mammalian cells by eosinophil cationic protein. *Eur. J. Biochem.* 269:307–316.

42. Mulloy, B., and E. A. Johnson. 1987. Assignment of the 1H-n.m.r. spectra of heparin and heparan sulphate. *Carbohydr. Res.* 170:151–165.

43. Ramos, A., P. Bayer, and G. Varani. 1999-2000. Determination of the structure of the RNA complex of a double-stranded RNA-binding domain from *Drosophila* Staufen protein. *Biopolymers.* 52:181–196.

44. Ramos, A., S. Grünert, …, G. Varani. 2000. RNA recognition by a Staufen double-stranded RNA-binding domain. *EMBO J.* 19:997–1009.

45. Torrent, M., M. V. Nogués, and E. Boix. Eosinophil cationic protein (ECP) can bind heparin and other glycosaminoglycans through its RNase active site. *J. Mol. Recognit.* In press.

46. Rubin, J., U. Zagai, …, P. Venge. 2009. The coding ECP 434(G>C) gene polymorphism determines the cytotoxicity of ECP but has minor effects on fibroblast-mediated gel contraction and no effect on RNase activity. *J. Immunol.* 183:445–451.

47. Gandhi, N. S., and R. L. Mancera. 2008. The structure of glycosaminoglycans and their interactions with proteins. *Chem. Biol. Drug Des.* 72:455–482.

48. Torrent, M., V. M. Nogués, and E. Boix. 2009. A theoretical approach to spot active regions in antimicrobial proteins. *BMC Bioinformatics.* 10:373.

49. Porcelli, F., R. Verardi, …, G. Veglia. 2008. NMR structure of the cathelicidin-derived human antimicrobial peptide LL-37 in dodecylphosphocholine micelles. *Biochemistry.* 47:5565–5572.

50. Lequin, O., F. Bruston, …, P. Nicolas. 2003. Helical structure of dermaseptin B2 in a membrane-mimetic environment. *Biochemistry.* 42:10311–10323.

51. Dubovskii, P. V., P. E. Volynsky, …, A. S. Arseniev. 2006. Spatial structure and activity mechanism of a novel spider antimicrobial peptide. *Biochemistry.* 45:10759–10767.

52. Vogt, B., P. Ducarme, …, B. Bechinger. 2000. The topology of lysine-containing amphipathic peptides in bilayers by circular dichroism, solid-state NMR, and molecular modeling. *Biophys. J.* 79:2644–2656.

53. Woschnagg, C., J. Rubin, and P. Venge. 2009. Eosinophil cationic protein (ECP) is processed during secretion. *J. Immunol.* 183: 3949–3954.

54. Ulrich, M., A. Petre, …, G. Döring. 2008. Post-translational tyrosine nitration of eosinophil granule toxins mediated by eosinophil peroxidase. *J. Biol. Chem.* 283:28629–28640.

55. Iwasaki, W., K. Nagata, …, F. Inagaki. 1997. Solution structure of midkine, a new heparin-binding growth factor. *EMBO J.* 16:6936–6946.

56. Spivak-Kroizman, T., M. A. Lemmon, …, I. Lax. 1994. Heparin-induced oligomerization of FGF molecules is responsible for FGF receptor dimerization, activation, and cell proliferation. *Cell.* 79: 1015–1024.

57. Fuchs, S. M., and R. T. Raines. 2006. Internalization of cationic peptides: the road less (or more?) traveled. *Cell. Mol. Life Sci.* 63:1819–1822.

58. Torrent, M., S. Navarro, …, E. Boix. 2008. Eosinophil cationic protein high-affinity binding to bacteria-wall lipopolysaccharides and peptidoglycans. *Biochemistry.* 47:3544–3555.